


## COMPARISON OF THE METHYLENE BLUE DYE REMOVAL ABILITY OF MAGNETIC MATERIALS SYNTHESIZED FROM VARIOUS TYPES OF FRUIT PEELS

ThanhThuy Tran <sup>\*</sup>, ThanhNha Tran, AnhThi Hoang, VanTrong Nguyen

<sup>a</sup>Faculty of Chemical Engineering, Industrial University of HCM City,  
Nguyen Van Bao str., HCM City, 70000, Vietnam

<sup>\*</sup>e-mail: [tranthithanhthuy@iu.edu.vn](mailto:tranthithanhthuy@iu.edu.vn)

**Abstract.** This study involved the synthesis of magnetic materials derived from pomelo peel (PP@Fe<sub>3</sub>O<sub>4</sub>), durian peel (DP@Fe<sub>3</sub>O<sub>4</sub>), and banana peel (BP@Fe<sub>3</sub>O<sub>4</sub>). The characteristics of these materials were examined using SEM, FTIR, XRD, and BET techniques. The adsorption parameters for methylene blue using these magnetic materials, including pH, material concentration, and adsorption duration, were investigated to optimise adsorption efficiency. Results indicated that the most effective material amounts were 0.09 g, 0.18 g, and 0.06 g for PP@Fe<sub>3</sub>O<sub>4</sub>, DP@Fe<sub>3</sub>O<sub>4</sub>, and BP@Fe<sub>3</sub>O<sub>4</sub>, respectively, in 25 mL of methylene blue solution, corresponding to concentrations of 3.6 g/L, 7.2 g/L, and 2.4 g/L. Similarly, the optimal pH values for adsorption were found to be 5.9, 7.7, and 7.4, while the most efficient adsorption times were determined to be 95.3, 42.2, and 128.4 minutes, respectively. Under these conditions, the highest methylene blue adsorption efficiencies achieved were 97.7%, 97%, and 98.9%, respectively. These materials were also employed to assess the chemical oxygen demand index in select water samples.

**Keywords:** bio-magnetic adsorbent, sustainable technology, fruit peel waste utilization.

Received: 31 January 2025/ Revised final: 28 April 2025/ Accepted: 2 May 2025

---

### Introduction

In today's modernized world, the advancement of industries like textiles, food processing, and chemical manufacturing has resulted in the release of significant volumes of waste into aquatic environments, particularly organic dyes. These dyes act as agents that diminish dissolved oxygen levels in water, posing substantial impacts on both organisms and human health. Various methods, including chemical, biological, and physical approaches, are employed to address organic dye pollutants [1]. However, each method exhibits distinct efficiency, requirements, and constraints. While chemical techniques, photocatalysis, and electrochemical methods are proficient in treating organic dyes, they often generate by-products that lead to secondary pollution. Environmentally sustainable biological methods necessitate stringent implementation conditions. Consequently, adsorption techniques, nanofiltration membranes, and coagulation processes have gained popularity due to their practicality, adaptability, cost-effectiveness, and eco-friendly outcomes.

Recently, there has been a surge in research exploring the utilization of fruit peels to fabricate adsorbent materials for organic dyes. These include orange peel [2,3], grapefruit peel [4,5], banana peel [6-8], apple peel [9,10], pineapple peel [11,12], durian peel [13-15], dragon fruit peel [16-19], coconut husk [20-22], watermelon peel [23,24], and mangosteen peel [25,26]. Various fruit peels are used to synthesize materials for adsorbing organic dyes due to the presence of compounds such as phenolic compounds, betalain, betacyanin with functional groups capable of adsorption such as C=C, C=O, O-H, N-H [16,27]. Most studies have involved preliminary treatment or carbonization of materials to enhance their adsorption capacity, with limited focus on material modification to further improve adsorption capacity.

Therefore, this study aims to compare the methylene blue adsorption capacity of magnetic materials synthesized from different fruit peels such as pomelo, durian, and banana. Magnetic materials enhance the efficiency of organic dye adsorption by combining adsorption capability

with magnetic properties, while the use of agricultural waste as raw materials contributes to minimizing environmental pollution caused by the impact of these types of waste. The effectiveness of organic dye removal in water samples was evaluated through the chemical oxygen demand (COD) in samples before and after adsorption using magnetic materials under optimal conditions. This method was applied to evaluate COD in water samples in some provinces in southern Vietnam.

## Experimental

### Materials

All chemicals used were of analytical grade, including methylene blue, iron(II) sulphate heptahydrate ( $\text{FeSO}_4 \cdot 7\text{H}_2\text{O}$ ), iron(III) chloride hexahydrate ( $\text{FeCl}_3 \cdot 6\text{H}_2\text{O}$ ), potassium dichromate ( $\text{K}_2\text{Cr}_2\text{O}_7$ ), ammonium iron(II) sulphate hexahydrate ( $[(\text{NH}_4)_2\text{Fe}(\text{SO}_4)_2 \cdot 6\text{H}_2\text{O}]$ ),  $\text{H}_2\text{SO}_4$ , and various other reagents. Experimental solutions were prepared using deionized water.

### Instruments

The analysis of material morphology was conducted with the use of a scanning electron microscope FE-SEM S4800 (Hitachi, Japan), operating at an accelerating voltage of 10.0 kV. The crystalline phase composition was assessed through X-ray powder diffraction using a Bruker D2 Phaser diffractometer equipped with  $\text{CuK}\alpha$  radiation. The molecular structure examination was performed *via* Fourier Transform Infrared Spectroscopy (Bruker, Germany). The surface area (BET) of the magnetic materials was evaluated with the Quantachrome High-Speed Gas Sorption Analyzer NOVA 3000 series (Model N32-11), and the concentration of methylene blue was determined by employing the Cary 3500 Compact UV-Vis spectrophotometer, measuring absorbance at a wavelength of 665 nm.

### Methods

#### Synthesis and characterization of materials

Various fruit peels, including pomelo (PP), durian (DP), and banana (BP), were cut into small pieces, dried for 48 hours, and then heated at 80°C for 24 hours before being ground into a fine powder (raw materials).

The magnetic materials were synthesized as follows [28]: A mixture of 4.08 g  $\text{FeSO}_4 \cdot 7\text{H}_2\text{O}$  and 4.74 g  $\text{FeCl}_3 \cdot 6\text{H}_2\text{O}$  in 100 mL distilled water was stirred at 70°C for 1 hour. Subsequently, 5.0 g of each type of raw material mentioned above was added to the mixture and stirred for 30 minutes. Sodium hydroxide (0.5M) was gradually added until the pH of the mixture reached 11 and stirring continued for 2 hours.

The precipitate was separated by a magnet, washed with distilled water until it reached a pH of 7.0, and then dried at 80°C for 5 hours. The resulting magnetic materials included pomelo peel magnetic material ( $\text{PP@Fe}_3\text{O}_4$ ), durian peel magnetic material ( $\text{DP@Fe}_3\text{O}_4$ ), and banana peel magnetic material ( $\text{BP@Fe}_3\text{O}_4$ ).

The properties of a material was determined by suitable methods, such as the equipment mentioned above.

#### Box-Behnken experimental design and parameter optimization

The Box-Behnken design (BBD) was employed to evaluate the MB adsorption capacity of three magnetic materials:  $\text{DP@Fe}_3\text{O}_4$ ,  $\text{PP@Fe}_3\text{O}_4$ , and  $\text{BP@Fe}_3\text{O}_4$  [29,30]. The experimental design included three independent factors: pH, adsorbent mass (g), and interaction time (minutes). Each factor was coded at three levels (-1, 0, +1). For the pH factor, the experimental conditions corresponded to values of 7, 8, and 9 for  $\text{DP@Fe}_3\text{O}_4$  and  $\text{BP@Fe}_3\text{O}_4$ , and 5, 6, and 7 for  $\text{PP@Fe}_3\text{O}_4$ . For the adsorbent mass, the designed experimental values were 0.1, 0.15, and 0.2 g for  $\text{DP@Fe}_3\text{O}_4$ , and 0.05, 0.075, and 0.1 g for both  $\text{PP@Fe}_3\text{O}_4$  and  $\text{BP@Fe}_3\text{O}_4$ . Lastly, the interaction time was set at 30, 45, and 60 minutes for  $\text{DP@Fe}_3\text{O}_4$ ; 90, 105, and 120 minutes for  $\text{PP@Fe}_3\text{O}_4$ ; and 120, 135, and 150 minutes for  $\text{BP@Fe}_3\text{O}_4$ . Each experiment was repeated 15 times for each material in 25 mL of MB solution at an initial concentration of 100 mg/L. A second-order regression model was used for statistical analysis to determine the optimal adsorption efficiency for each material. The model's goodness of fit was evaluated using  $R^2$  values, and statistical significance was assessed using ANOVA, with  $p < 0.05$  considered significant.

#### Methylene blue adsorption process and evaluation of organic dye treatment ability

The methylene blue (MB) adsorption process was investigated as follows: 25 mL of MB solution with a concentration of 100 mg/L was added to a beaker; the amount of adsorbent material, adsorption time, and pH of the solution (using previously determined optimal values) were adjusted with constant agitation at 175 rpm. The absorbance of the MB solution was measured at a wavelength of 665 nm. The calibration curve for MB concentration measurement was established using standard solutions in the range of 0.5–10.0 mg/L. The linear equation obtained was  $A = 0.1727C + 0.002$ , with an  $R^2$  value of 0.9998, ensuring accuracy in concentration determination.

The MB adsorption efficiency of the materials was evaluated based on the concentration of MB solution before and after adsorption.

The procedure for determining the chemical oxygen demand (*COD*) value and evaluating the ability to remove organic dyes in water samples was as follows: 25 mL of MB was added to a 250 mL beaker, followed by adsorption according to the previously investigated procedure. The adsorbent was separated by a magnet, and the solution after adsorption was collected. The *COD* value in the solution after adsorption was accurately determined using the dichromate method following APHA Standard Methods 5220C. Closed Reflux, Titrimetric Method, 2017 [31].

The *COD* value was calculated according to Eq.(1).

$$COD = \frac{(V_0 - V) \times C_N \times 8000}{V_m} * F \text{ (mgO}_2\text{/L)} \quad (1)$$

where,  $V_0$  - the volume of  $K_2Cr_2O_7$  used to determine the blank sample (mL);

$V$  - the volume of  $K_2Cr_2O_7$  used to determine the sample (mL);

$V_m$  - the volume of sample (mL);

$C_N$  - the concentration of  $K_2Cr_2O_7$  (N);

$F$  - the dilution factor.

Water samples were collected from various locations in the provinces of Tien Giang and Long An, filtered through a 0.22  $\mu\text{m}$  membrane, and adjusted to  $\text{pH} \leq 7$  before use. The process of organic dye adsorption using the materials and *COD* value evaluation of water samples was conducted following the above method.

## Results and discussion

The adsorption efficiency of magnetic materials synthesized from pomelo, durian, and banana peels for methylene blue was investigated. The results demonstrated that the magnetic material derived from banana peel exhibited the highest adsorption performance.

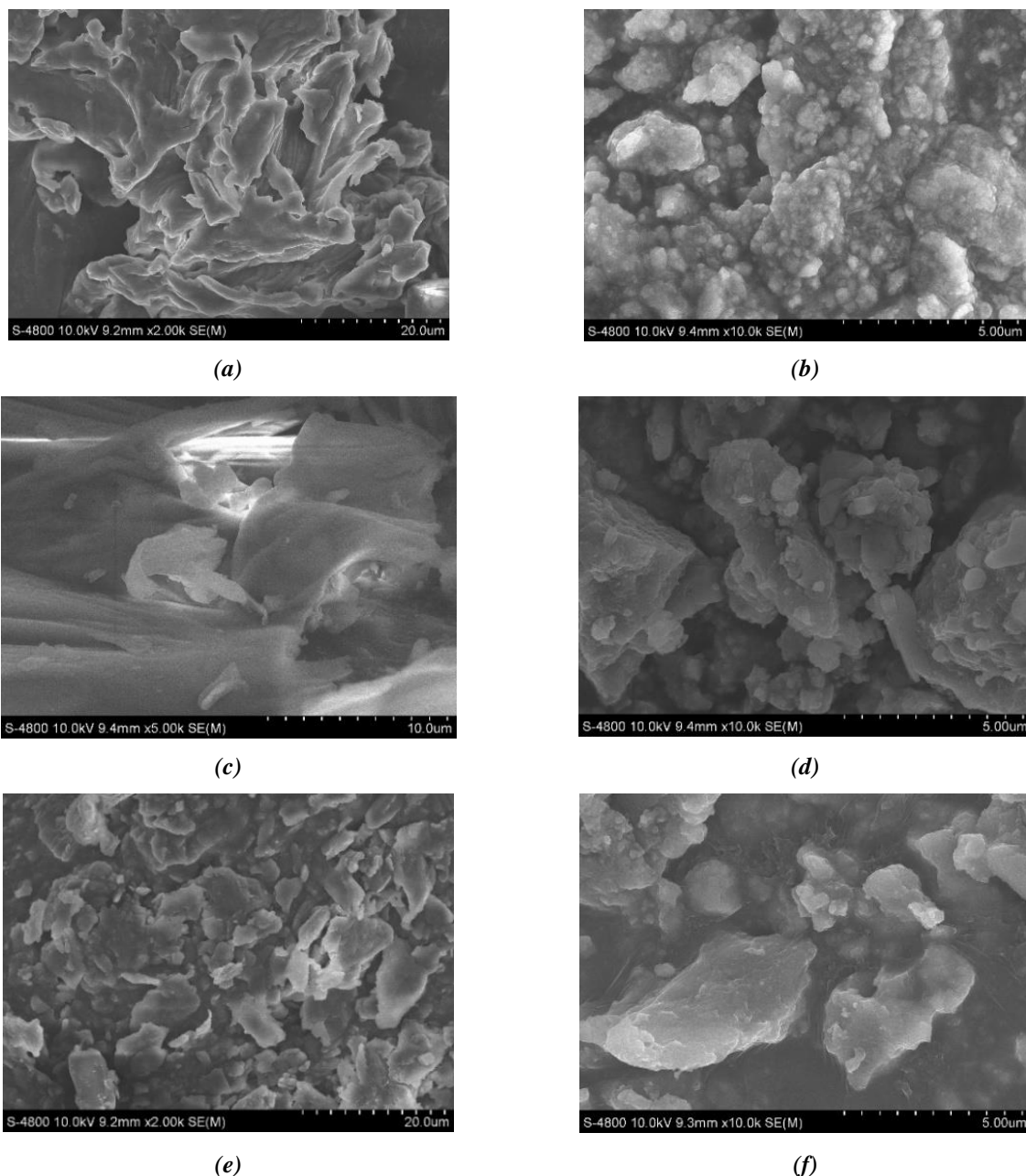
### Characterization of the materials

Figure 1 illustrates the magnetic materials synthesized from different types of peels. Figure 1(a) displays the magnetic material derived from pomelo peel ( $\text{PP@Fe}_3\text{O}_4$ ), while Figure 1(b) showcases the magnetic material from durian peel ( $\text{DP@Fe}_3\text{O}_4$ ), and Figure 1(c) represents the magnetic material sourced from banana peel ( $\text{BP@Fe}_3\text{O}_4$ ).



**Figure 1. The synthesised materials  $\text{PP@Fe}_3\text{O}_4$  (a),  $\text{DP@Fe}_3\text{O}_4$  (b) and  $\text{BP@Fe}_3\text{O}_4$  (c).**

Figure 2 illustrates the surface morphology of the materials. Figure 2(a) shows the highly porous microstructure of the pomelo peel, which is comparable with the published result [32]. For durian peel material (Figure 2 (b)), the surface morphology exhibits a non porous configuration, which is consistent with previous publication [33]. And Figure 2(c) shows that the banana peel material has a particulate structure with micro-sized dimensions, which is also consistent with previous publications [34]. Following modification with  $\text{Fe}_3\text{O}_4$ , all materials (Figure 2(b),(d),(f)) show modified surface structures, characterised by increased porosity compared to the raw materials (Figure 2(a) (c),(e)). This suggests the presence of  $\text{Fe}_3\text{O}_4$  magnetic nanoparticles on the raw materials derived from pomelo peel, durian peel, and banana peel. The porous surface structure of the magnetic materials enhances the contact area with MB molecules, thus improving adsorption efficiency. This observation is supported by the adsorption results discussed in the following section.



**Figure 2.** SEM images of the materials PP (a) and PP@Fe<sub>3</sub>O<sub>4</sub> (b), DP (c) and DP@Fe<sub>3</sub>O<sub>4</sub> (d), BP (e) and BP@Fe<sub>3</sub>O<sub>4</sub> (f).

The FT-IR spectra displayed in Figure 3 depict the materials before and after MB adsorption. In this figure, the black lines represent the spectra of PP (a), DP (b), and BP (c), while the red lines correspond to the spectra of the synthesized magnetic materials PP@Fe<sub>3</sub>O<sub>4</sub> (a), DP@Fe<sub>3</sub>O<sub>4</sub> (b), and BP@Fe<sub>3</sub>O<sub>4</sub> (c). The blue lines indicate the spectra of these materials after MB adsorption, labelled as PP@Fe<sub>3</sub>O<sub>4</sub>\_MB (a), DP@Fe<sub>3</sub>O<sub>4</sub>\_MB (b), and BP@Fe<sub>3</sub>O<sub>4</sub>\_MB (c). Before MB adsorption, the FTIR spectra of PP@Fe<sub>3</sub>O<sub>4</sub> (a), DP@Fe<sub>3</sub>O<sub>4</sub> (b), and BP@Fe<sub>3</sub>O<sub>4</sub> (c) exhibit characteristic peaks at approximately 3388 cm<sup>-1</sup>, 3384 cm<sup>-1</sup>, and 3404 cm<sup>-1</sup>, respectively, which correspond to the stretching vibrations

of –OH groups derived from lignin and cellulose present in the shell materials. Peaks at 2933 cm<sup>-1</sup> for PP, 2923 cm<sup>-1</sup> for DP, and 2922 cm<sup>-1</sup> for BP are attributed to the stretching vibrations of saturated C–H bonds, which are components of cellulose and lignin in all three peels. Additionally, characteristic peaks associated with C–O and C–O–C stretching vibrations from carboxylic acids, phenols, alcohols, or esters appear at 1313 cm<sup>-1</sup>, 1336 cm<sup>-1</sup>, and 1326 cm<sup>-1</sup>, as well as at 1055 cm<sup>-1</sup>, 1074 cm<sup>-1</sup>, and 1022 cm<sup>-1</sup>, respectively. Furthermore, peaks observed at 1645 cm<sup>-1</sup> and 1746 cm<sup>-1</sup> in PP, 1643 cm<sup>-1</sup> and 1741 cm<sup>-1</sup> in DP, and 1641 cm<sup>-1</sup> and 1735 cm<sup>-1</sup> in BP correspond to C=O stretching vibrations from carboxylic acids

and esters [16,40,41]. The presence of peaks in the 2320–2378  $\text{cm}^{-1}$  range in the spectra may indicate  $\text{C}\equiv\text{C}$  stretching vibrations from alkyne group [35,36]. However, this signal is unexpected in the materials and may result from partial carbonization of organic components during synthesis. After MB adsorption, noticeable changes in the characteristic peaks and their intensities are observed. The variations in intensity and position of functional groups associated with alcohols and phenols in the 3300–3500  $\text{cm}^{-1}$  range suggest interactions with MB. Peaks around 1500–1600  $\text{cm}^{-1}$ , possibly related to amine and aromatic ring vibrations, and peaks in the 1600–1700  $\text{cm}^{-1}$  region, potentially associated with  $-\text{CH}=\text{N}$  functional groups, indicate possible interactions between MB and the material surface.

The X-ray diffraction (XRD) results of the  $\text{Fe}_3\text{O}_4$  nanoparticles and magnetic materials are shown in Figure 4. The characteristic peaks of  $\text{Fe}_3\text{O}_4$  appear at  $2\theta$  angles around  $30.2^\circ$ ,  $35.5^\circ$ ,  $43.2^\circ$ ,  $53.5^\circ$ ,  $57.2^\circ$ , and  $66.2^\circ$ , corresponding to the crystal planes (311), (400), (422), (511), and (440), according to JCPDs No. 19-0629 and previously published studies [37,38]. The XRD spectra of the composite materials,  $\text{PP@Fe}_3\text{O}_4$ ,  $\text{DP@Fe}_3\text{O}_4$ , and  $\text{BP@Fe}_3\text{O}_4$ , also showed the presence of  $\text{Fe}_3\text{O}_4$  peaks. However, the signal intensity of the  $\text{Fe}_3\text{O}_4$  peaks in the composite samples is significantly lower than that of the pure  $\text{Fe}_3\text{O}_4$  nanoparticles. This can be explained by the SEM morphology results, which show that  $\text{Fe}_3\text{O}_4$  is well dispersed on the surface of the raw materials.

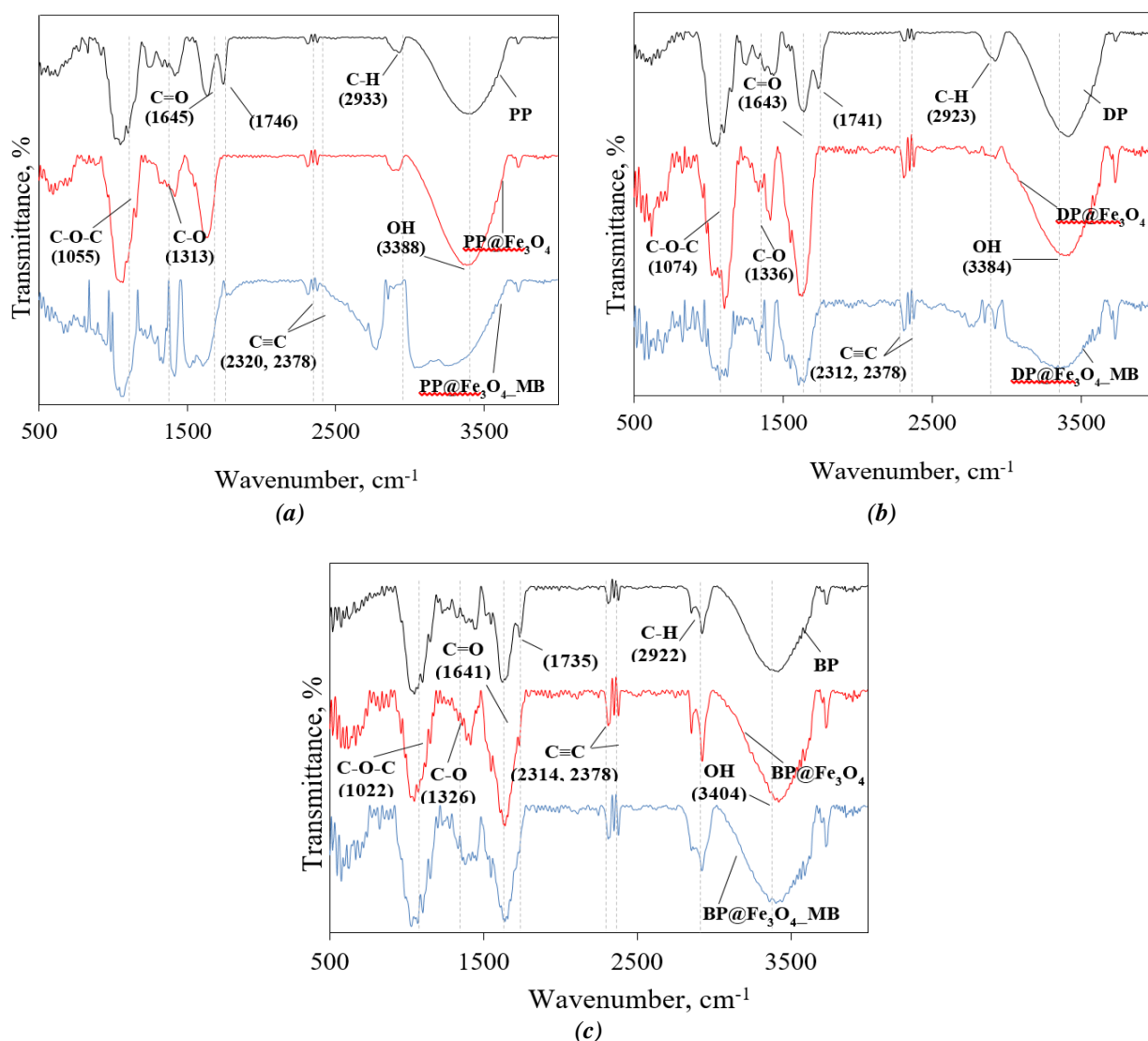


Figure 3. FT-IR spectra of the absorbent derived from pomelo (a), durian (b), and banana (c) peels.



This good dispersion, as observed by SEM, may lead to an increase in the amorphous phase in the material, which consequently reduces the intensity of the  $\text{Fe}_3\text{O}_4$  peaks in the XRD patterns (Figure 4). Additional possible explanations for this phenomenon include small particle size and poor crystallinity. This result is consistent with a previous publication [39], where low  $\text{Fe}_3\text{O}_4$  peak intensities were observed in the [magnetic graphene oxide/ $\text{Fe}_3\text{O}_4$ /banana peel] composite sample.

Table 1 presents the findings regarding the surface area (BET) of the materials. These findings suggest a notable increase in the surface area due to the presence of  $\text{Fe}_3\text{O}_4$  on raw materials. Specifically, the surface area increased from  $0.03 \text{ m}^2/\text{g}$  to  $1.32 \text{ m}^2/\text{g}$  for  $\text{PP@Fe}_3\text{O}_4$ , from  $1.51 \text{ m}^2/\text{g}$  to  $3.66 \text{ m}^2/\text{g}$  for  $\text{DP@Fe}_3\text{O}_4$ , and from  $1.86 \text{ m}^2/\text{g}$  to  $5.63 \text{ m}^2/\text{g}$  for  $\text{BP@Fe}_3\text{O}_4$ . This increase can be explained by the good dispersion of  $\text{Fe}_3\text{O}_4$  particles on the surface of the raw materials, creating more active sites for the adsorption process. The pore volume and pore size also experienced significant changes. The pore volume increased from  $0.001 \text{ cm}^3/\text{g}$  to

$0.005 \text{ cm}^3/\text{g}$  for  $\text{PP@Fe}_3\text{O}_4$ , from  $0.280 \text{ cm}^3/\text{g}$  to  $0.533 \text{ cm}^3/\text{g}$  for  $\text{DP@Fe}_3\text{O}_4$ , and  $0.679 \text{ cm}^3/\text{g}$  for  $\text{BP@Fe}_3\text{O}_4$ . The pore size also varied, with  $\text{PP@Fe}_3\text{O}_4$  having a pore size of  $72.14 \text{ nm}$ ,  $\text{DP@Fe}_3\text{O}_4$  having a pore size of  $1146.04 \text{ nm}$ , and  $\text{BP@Fe}_3\text{O}_4$  having a pore size of  $9.86 \text{ nm}$ . This variation indicates the formation of new pore structures, which may affect the adsorption capacity of MB molecules of different sizes. Although the data for the raw materials (PP, DP, BP) were taken from [40-42], due to resource limitations, there may be differences from experimental data. However, this result still shows that the magnetic materials have significantly larger surface area, pore volume, and pore size compared to the raw materials. This indicates that magnetic materials have great potential in adsorbing MB molecules. The experimental results in Table 1 have shown that the adsorption capacity of magnetic materials is much larger than that of raw materials. Thus, it can be inferred that magnetic materials characterised by substantial surface area, pore volume, and pore size are advantageous for the adsorption of MB molecules.

Table 1

Surface area of materials.				
Materials	Surface area ( $\text{m}^2/\text{g}$ )	Pore volume ( $\text{cm}^3/\text{g}$ )	Pore size (nm)	References
PP	0.03	0.001	-	[40]
$\text{PP@Fe}_3\text{O}_4$	1.32	0.005	72.14	This study
DP	1.51	0.280	3660.00	[41]
$\text{DP@Fe}_3\text{O}_4$	3.66	0.533	1146.04	This study
BP	1.86	-	1.53	[42]
$\text{BP@Fe}_3\text{O}_4$	5.63	0.679	9.86	This study

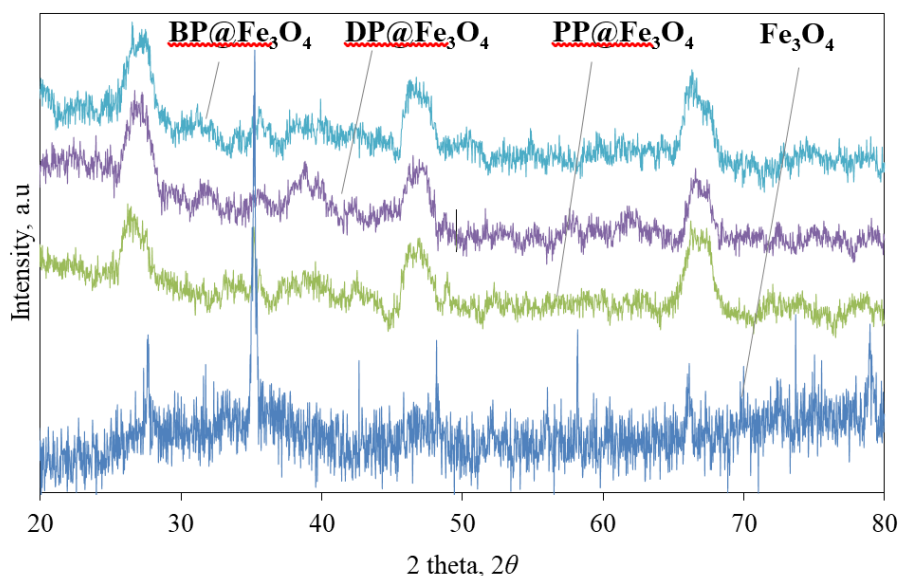


Figure 4. XRD patterns of magnetic materials synthesized from fruit peels.

### Factors affecting the adsorption efficiency of MB pH

The outcomes depicted in Figure 5(a) reveal that fruit peels, comprising natural constituents like cellulose, lignin, etc., containing  $-\text{OH}$ , and  $-\text{C}=\text{O}$  functional groups, can be protonated under acidic conditions. Moreover, in a low-pH environment,  $\text{H}^+$  ions compete with MB for adsorption sites, resulting in a reduction in available sites. With the pH rising from 3 to 9, the material's adsorption efficiency gradually rises and stabilizes, followed by a slight decline at pH 11 due to cation exchange between MB molecules and the material surface. For the  $\text{PP@Fe}_3\text{O}_4$  material, as pH escalates from 5 to 7, adsorption efficiency fluctuates between 86.3% and 94.9%. Conversely, for  $\text{DP@Fe}_3\text{O}_4$ , efficiency varies between 91.2% and 93.1% as pH increases from 7 to 9. Likewise, for  $\text{BP@Fe}_3\text{O}_4$ , the efficiency ranges from 98.5% to 98.7% as pH elevates from 7 to 9. Consequently, pH values ranging from 5 to 7 and 7 to 9 are selected to determine the optimal pH for methylene blue adsorption using  $\text{PP@Fe}_3\text{O}_4$ ,  $\text{DP@Fe}_3\text{O}_4$ ,  $\text{BP@Fe}_3\text{O}_4$  materials, employing the Box-Behnken experimental design model.

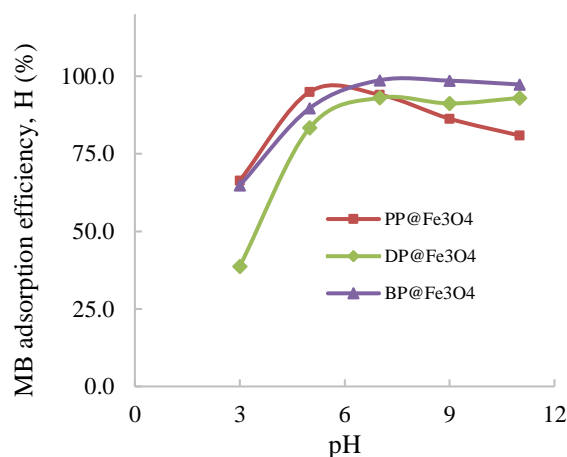
### Material mass

The variation in material mass leads to changes in the mass and surface area of the material exposed to MB, directly affecting the adsorption efficiency. The effect of material mass was investigated in the range of 0.01 to 0.30 g using 25 mL of MB solution at a concentration of 100 mg/L, while maintaining constant other optimal parameters. The results presented in Figure 5(b) demonstrate that the adsorption efficiency increases gradually with the increase in material mass. This could be attributed to the increased availability of adsorption sites on the material surface after it combines with iron nanoparticles, allowing the material to interact with MB molecules more effectively, thus leading to an increase in adsorption efficiency. For the  $\text{PP@Fe}_3\text{O}_4$ ,  $\text{DP@Fe}_3\text{O}_4$ , and  $\text{BP@Fe}_3\text{O}_4$  materials, when using increasing material masses from 0.02 g to 0.20 g, the corresponding adsorption efficiencies increase from 70.0% to 99.5%. Therefore, material masses ranging from 0.02 g to 0.20 g were chosen for further investigation of the simultaneous impact of multiple factors across different material types.

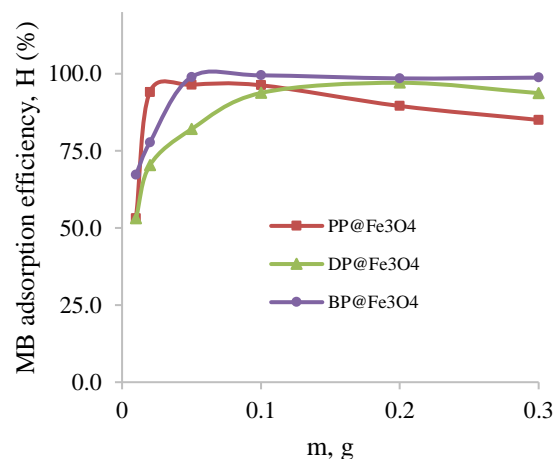
### Adsorption time

One of the factors investigated is adsorption time, which was explored within the range of 1 to 180 minutes while keeping other optimal

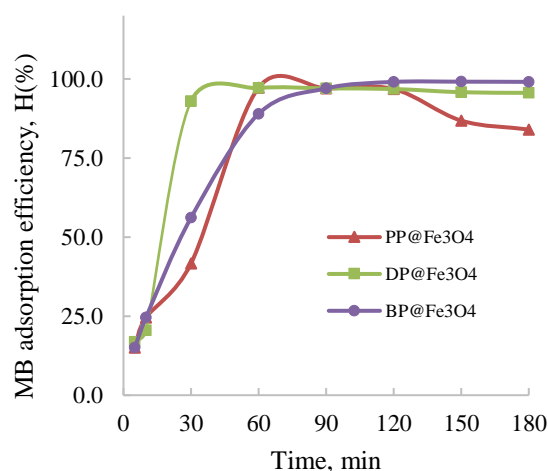
parameters constant. The results presented in Figure 5(c) show that the adsorption efficiency of the materials increases gradually with increasing time.



(a)



(b)



(c)

**Figure 5. Effect of pH (a), material mass (b), and adsorption time (c) of magnetic materials.**

The absorption of the materials mainly occurs in two stages. The first stage occurs rapidly within the first 90 minutes, as there are many adsorption sites on the material surface facilitating the diffusion of MB onto the material surface more easily. The second stage occurs when both the adsorption and desorption processes take place simultaneously due to the limited availability of adsorption sites. During this stage, the interaction between MB and the material weakens due to saturation of adsorption sites, and this process continues until reaching equilibrium after a certain period. For the PP@Fe<sub>3</sub>O<sub>4</sub> material, adsorption efficiency ranges between 87.9% and 97.0% as time increases from 60 to 120 minutes. Similarly, the adsorption efficiency of the DP@Fe<sub>3</sub>O<sub>4</sub> material varies between 86.8% and 97.1% as time increases from 30 to 90 minutes. Finally, adsorption efficiency varies between 89.1% and 99.1% as time increases from 60 to 150 minutes for the BP@Fe<sub>3</sub>O<sub>4</sub> material. Consequently, the time range from 30 to 150 minutes was selected to investigate the simultaneous impact of multiple factors across different material types.

#### *Optimal parameters for the adsorption process*

To determine the optimal MB adsorption conditions using fruit peel-derived magnetic materials, a Box-Behnken experimental design was employed. The obtained optimal parameters and corresponding MB adsorption efficiencies are presented in Table 2.

The results demonstrate a high correlation between the predicted and experimental adsorption

efficiencies, with deviations of 0.5%, 0.1%, and 0.2% for PP@Fe<sub>3</sub>O<sub>4</sub>, DP@Fe<sub>3</sub>O<sub>4</sub>, and BP@Fe<sub>3</sub>O<sub>4</sub>, respectively, all within the acceptable range (<5%) [14]. This correlation is further supported by the high coefficients of determination ( $R^2$ ) for the quadratic regression models: 0.9871 (PP@Fe<sub>3</sub>O<sub>4</sub>), 0.9930 (DP@Fe<sub>3</sub>O<sub>4</sub>), and 0.9983 (BP@Fe<sub>3</sub>O<sub>4</sub>), indicating a strong relationship between the experimental data and the predicted responses. ANOVA analysis also confirmed the statistical significance of the models ( $p < 0.05$ ), validating the reliability of the regression equations for predicting adsorption efficiency.

#### *Isothermal adsorption model*

The experimental data in Table 3 suggests that the Langmuir isothermal model is more suitable for the MB adsorption process, indicated by the higher linear correlation coefficient  $R^2$  compared to the Freundlich model. This implies that MB adsorbs onto a homogeneous surface of the material in a single layer. Additionally, the calculated RL values, falling within the range of 0.01 to 0.90 ( $0 < R_L < 1$ ) for both raw and magnetic embedded materials, suggest favourable adsorption onto the material surface. The Freundlich model also supports the favourable adsorption process, with the  $n$  coefficient ranging from 1.56 to 2.94 ( $1 < n < 10$ ). Furthermore, both models demonstrate an enhancement in the maximum adsorption capacity of magnetic materials compared to raw materials.

Table 2

**Optimal parameters for the MB adsorption process.**

No.	Materials	pH	Material's mass (g)	Time (min)	Absorption efficiency (%)	
					Predicted	Experimental
1	PP@Fe <sub>3</sub> O <sub>4</sub>	5.9	0.09	95.3	97.2	97.7
2	DP@Fe <sub>3</sub> O <sub>4</sub>	7.7	0.18	42.2	96.9	97.0
3	BP@Fe <sub>3</sub> O <sub>4</sub>	7.4	0.06	128.4	99.1	98.9

Table 3

**Parameters of the Langmuir and Freundlich isothermal models.**

	Langmuir parameters			Freundlich parameters		
	$q_{max}$ (mg/g)	$K_L$ (L/mg)	$R^2$	$K_f$ (mg/g.(L/mg) <sup>1/n</sup> )	1/n	$R^2$
PP	27.43	0.20	0.988	5.4	0.34	0.792
PP@Fe <sub>3</sub> O <sub>4</sub>	44.73	0.35	0.978	7.4	0.39	0.869
DP	42.20	0.03	0.98	1.8	0.62	0.988
DP@Fe <sub>3</sub> O <sub>4</sub>	60.13	0.08	0.938	4.7	0.62	0.984
BP	84.82	0.02	0.929	2.8	0.64	0.987
BP@Fe <sub>3</sub> O <sub>4</sub>	205.69	0.17	0.949	26.4	0.53	0.903



The MB adsorption capacity of magnetic materials is compared with the results from some other previous publications in Table 4.

#### Selective adsorption efficiency of the materials

The selective adsorption experiment was conducted with a mixture of methylene blue (MB), methylene green (MG), and rhodamine B (RhB) at a concentration of 100 mg/L under the optimized conditions of pH, material mass, and adsorption time as described above. The solution after adsorption was analysed using the UV-Vis method.

The results shown in Figure 6 demonstrate that the material exhibits high selectivity for MB, but it also can adsorb MG and RhB. This could be due to the similar molecular sizes of MB, MG, and RhB, and their cationic dye nature, allowing them to adsorb onto the material surface. These results indicate that magnetic materials can be applied to simultaneously adsorb various organic pollutants in water, hence evaluating the ability to treat organic dye pollutants in water through COD values is appropriate.

Table 4

**Comparison of MB adsorption capacity of magnetic materials with other reported adsorbents.**

Absorbent materials	Material's mass (g)	$Q_m$ (mg/g)	References
Magnetic potato peel	0.2g/10 mL	14.3	[28]
Magnetic mustard seed husk	0.024g/10 mL	44.61	[43]
Magnetic straw composite	1g/1000 mL	1374.6	[44]
Magnetic peanut shell	0.01g/10 mL	32.5	[45]
Magnetic bran composite	10g/1000 mL	150.53	[46]
Magnetic dragon fruit peel (DFP@Fe <sub>3</sub> O <sub>4</sub> )	0.02 g/25 mL	268.64	[19]
PP@Fe <sub>3</sub> O <sub>4</sub>	0.09g/25mL	44.73	This study
DP@Fe <sub>3</sub> O <sub>4</sub>	0.18g/25mL	60.13	This study
BP@Fe <sub>3</sub> O <sub>4</sub>	0.06g/25mL	205.69	This study

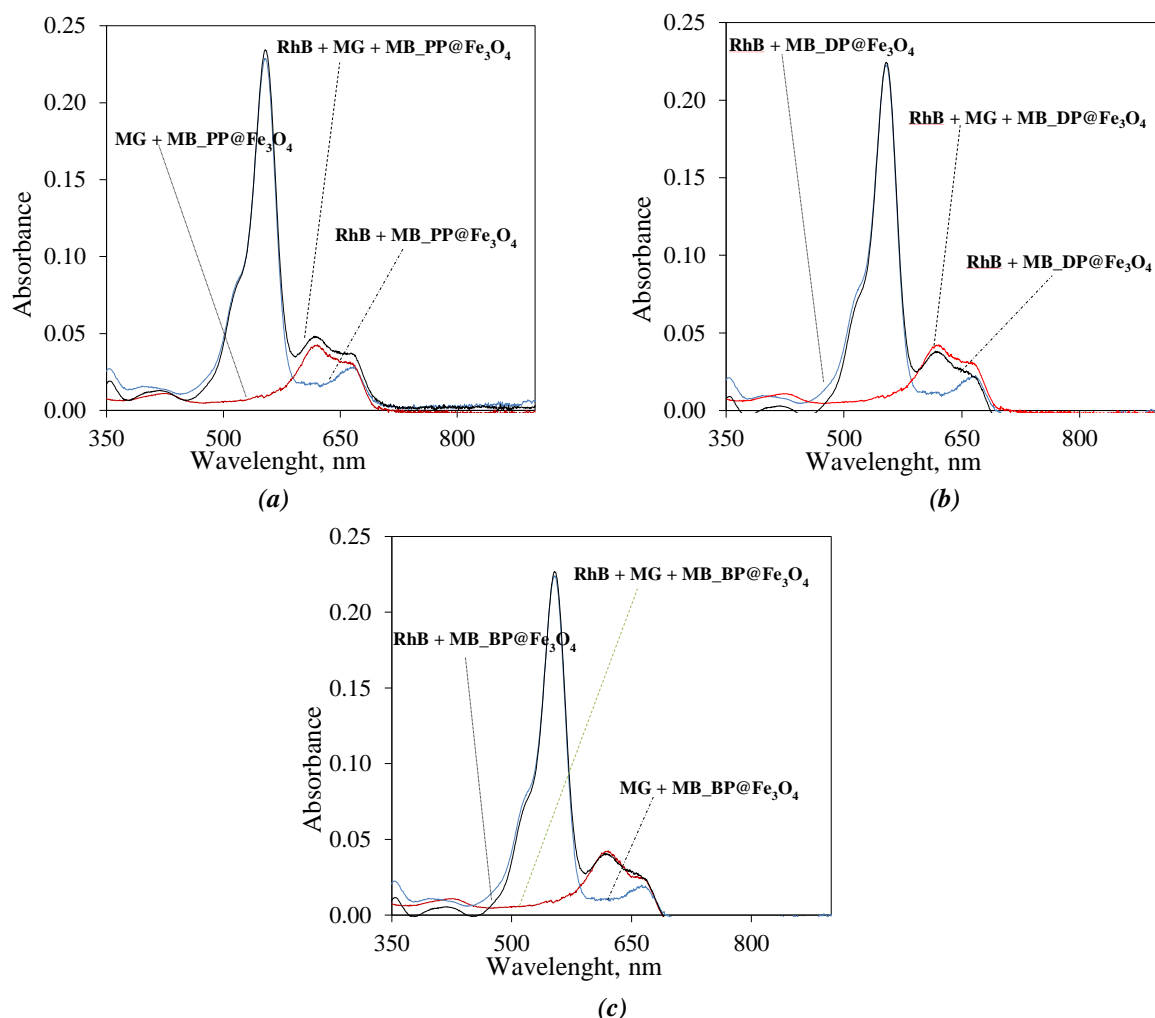


**Figure 6. Absorption spectra of the dye mixture after adsorption by the magnetic materials PP@Fe<sub>3</sub>O<sub>4</sub> (a), DP@Fe<sub>3</sub>O<sub>4</sub> (b) and BP@Fe<sub>3</sub>O<sub>4</sub> (c).**

Table 5

Treatment capacity of organic dyes in water samples by magnetic materials.				
Samples	Materials	$C_{MB}$ (mg/L)	COD (mgO <sub>2</sub> /L)	H (%)
MB	-	100	107	-
	PP@Fe <sub>3</sub> O <sub>4</sub>	100	4	96
	DP@Fe <sub>3</sub> O <sub>4</sub>	100	3	97
	BP@Fe <sub>3</sub> O <sub>4</sub>	100	2	99
	DFP@Fe <sub>3</sub> O <sub>4</sub>	100	8	93 [19]
RhB, MG (100mg/L)	-	100	306	-
	PP@Fe <sub>3</sub> O <sub>4</sub>	100	138	55
	DP@Fe <sub>3</sub> O <sub>4</sub>	100	92	70
	BP@Fe <sub>3</sub> O <sub>4</sub>	100	46	85
	DFP@Fe <sub>3</sub> O <sub>4</sub>	100	137	55 [19]
Water samples from the Tien River area (Tien Giang Province).	-	-	76	-
	-	100	168	92
	PP@Fe <sub>3</sub> O <sub>4</sub>	-	19	75
	DP@Fe <sub>3</sub> O <sub>4</sub>	-	15	80
	BP@Fe <sub>3</sub> O <sub>4</sub>	-	8	90
	DFP@Fe <sub>3</sub> O <sub>4</sub>	-	38	77 [19]
Water samples from fish ponds in Cho Gao district (Tien Giang Province).	-	-	80	-
	-	100	183	103
	PP@Fe <sub>3</sub> O <sub>4</sub>	-	15	81
	DP@Fe <sub>3</sub> O <sub>4</sub>	-	19	76
	BP@Fe <sub>3</sub> O <sub>4</sub>	-	4	95
	DFP@Fe <sub>3</sub> O <sub>4</sub>	-	27	85 [19]
Aquaculture water (Long An Province)	-	-	92	-
	-	100	199	107
	PP@Fe <sub>3</sub> O <sub>4</sub>	-	15	84
	DP@Fe <sub>3</sub> O <sub>4</sub>	-	11	88
	BP@Fe <sub>3</sub> O <sub>4</sub>	-	8	92
	DFP@Fe <sub>3</sub> O <sub>4</sub>	-	31	84 [19]

### Evaluation of the ability to treat organic dye pollutants in water samples

The ability to treat organic dye pollutants in water samples was assessed by determining the COD value of the sample before and after treatment with magnetic materials. The results are presented in Table 5.

Table 5 reveals that magnetic materials sourced from fruit peels exhibit significant efficacy in the treatment of organic dyes, as reflected by COD values. Magnetic materials derived from banana peels demonstrate superior efficiency in removing organic dyes from water samples, achieving a treatment range between 90% and 95%. BP@Fe<sub>3</sub>O<sub>4</sub> appears to possess the largest surface area, resulting in the highest absorption capacity among the materials examined.

### Conclusions

Magnetic materials synthesized from various fruit peels have been applied for the adsorption of methylene blue. Optimal adsorption conditions were investigated to achieve the highest adsorption efficiency ranging from 97.0% to

98.9%, with pH ranging from 5.9 to 7.7; optimal material mass ranging from 0.09 to 0.18 g; and optimal adsorption time ranging from 42.2 to 128.4 minutes for PP@Fe<sub>3</sub>O<sub>4</sub>, DP@Fe<sub>3</sub>O<sub>4</sub>, BP@Fe<sub>3</sub>O<sub>4</sub> materials, respectively. Although BP@Fe<sub>3</sub>O<sub>4</sub> exhibited the highest methylene blue adsorption efficiency, reaching 98.9%, with the lowest optimal amount of material (0.09 g), it also had the longest adsorption time. Therefore, the selection of materials needs to be considered both adsorption efficiency and adsorption kinetics. The magnetic materials were applied to assess their ability to treat organic dyes in water samples with high efficiency ranging from 75% to 95%, depending on the type of material and water sample. Future research should focus on optimizing the adsorption kinetics of BP@Fe<sub>3</sub>O<sub>4</sub>, evaluating the reusability of the materials, and expanding applications to other organic pollutants. The use of fruit peels for synthesizing adsorbent materials not only synthesis highly effective materials for methylene blue removal but also serves as a method for processing agricultural waste, helping to prevent environmental pollution.

## Acknowledgments

The authors are grateful to the Faculty of Chemical Engineering, Industrial University of Ho Chi Minh City for their support in providing facilities and equipment that helped complete this research. Additionally, the authors would like to thank the editorial board and reviewers for their valuable contributions in enhancing the quality of this article.

## References

1. Ashraf, R.S.; Abid, Z.; Shahid, M.; Rehman, Z.U.; Muhammad, G.; Altaf, M.; Raza, M.A. Methods for the treatment of wastewaters containing dyes and pigments. Inamuddin; Ahamed, M.I.; Lichtfouse, E. Eds. Water Pollution and Remediation: Organic pollutants. Springer: Cham, 2021, pp. 597–661. DOI: [http://doi.org/10.1007/978-3-030-52395-4\\_17](http://doi.org/10.1007/978-3-030-52395-4_17)
2. Al-Azabi, K.; Al-Marog, S.; Abukrain, A.; Sulyman, M. Equilibrium, isotherm studies of dye adsorption onto orange peel powder. Chemistry Research Journal, 2018, 3(1), pp. 45–59. <https://chemrj.org/download/vol-3-iss-1-2018/chemrj-2018-03-01-45-59.pdf>
3. Munagapati, V.S.; Wen, J.-C.; Pan, C.-L.; Gutha, Y.; Wen, J.-H. Enhanced adsorption performance of reactive red 120 azo dye from aqueous solution using quaternary amine modified orange peel powder. Journal of Molecular Liquids, 2019, 285, pp. 375–385. DOI: <https://doi.org/10.1016/j.molliq.2019.04.081>
4. Zhang, B.; Wu, Y.; Cha, L. Removal of methyl orange dye using activated biochar derived from pomelo peel wastes: performance, isotherm, and kinetic studies. Journal of Dispersion Science and Technology, 2020, 41(1), pp. 125–136. DOI: <https://doi.org/10.1080/01932691.2018.1561298>
5. Inkoua, S.; Maloko, H.L.; Koko, M.M.; Yan, L. Facile solvothermal synthesis of Fe<sub>3</sub>O<sub>4</sub>/magnetic grapefruit peel for adsorptive removal of congo red, humic acid and phosphate from aqueous solutions. Materials Express, 2020, 10(1), pp. 37–44. DOI: <https://doi.org/10.1166/mex.2020.1610>
6. Sahu, P.; Verma, S. Removal efficiency assessment of absorbent based on banana peel for methylene blue. International Journal of Applied Research, 2021, 7(9), pp. 171–174. [https://www.irjmets.com/uploadedfiles/paper/volume\\_3/issue\\_9\\_september\\_2021/16402/final/fin\\_irjmets1632755481.pdf](https://www.irjmets.com/uploadedfiles/paper/volume_3/issue_9_september_2021/16402/final/fin_irjmets1632755481.pdf)
7. Hashem, A.H.; Saied, E.; Hasanin, M.S. Green and ecofriendly bio-removal of methylene blue dye from aqueous solution using biologically activated banana peel waste. Sustainable Chemistry and Pharmacy, 2020, 18, pp. 100333. DOI: <https://doi.org/10.1016/j.scp.2020.100333>
8. Munagapati, V.S.; Wen, J.-C.; Pan, C.-L.; Gutha, Y.; Wen, J.-H.; Reddy, G.M. Adsorptive removal of anionic dye (Reactive black 5) from aqueous solution using chemically modified banana peel powder: kinetic, isotherm, thermodynamic, and reusability studies. International Journal of Phytoremediation, 2020, 22(3), pp. 267–278. DOI: <https://doi.org/10.1080/15226514.2019.1658709>
9. Enniya, I.; Jourani, A. Study of methylene blue removal by a biosorbent prepared with apple peels. Journal of Materials and Environmental Sciences, 2017, 8(12), pp. 4573–4581. DOI: <http://doi.org/10.26872/jmes.2017.8.12.883>
10. Bello, M.O.; Abdus-Salam, N.; Adekola, F.A.; Pal, U. Isotherm and kinetic studies of adsorption of methylene blue using activated carbon from ackee apple pods. Chemical Data Collections, 2021, 31, pp. 100607. DOI: <https://doi.org/10.1016/j.cdc.2020.100607>
11. Kamaru, A.A.; Sani, N.S.; Nik Malek, N.A.N. Raw and surfactant-modified pineapple leaf as adsorbent for removal of methylene blue and methyl orange from aqueous solution. Desalination and Water Treatment, 2016, 57(40), pp. 18836–18850. DOI: <https://doi.org/10.1080/19443994.2015.1095122>
12. Mahmud, K.N.; Wen, T.H.; Zakaria, Z.A. Activated carbon and biochar from pineapple waste biomass for the removal of methylene blue. Environmental and Toxicology Management, 2021, 1(1), pp. 30–36. DOI: <http://doi.org/10.33086/etm.v1i1.2036>
13. Thuong, N.T.; Nhi, N.T.T.; Nhung, V.T.C.; Bich, H.N.; Quynh, B.T.P.; Bach, L.G.; Trinh, N.D. A fixed-bed column study for removal of organic dyes from aqueous solution by pre-treated durian peel waste. Indonesian Journal of Chemistry, 2019, 19(2), pp. 486–494. DOI: <http://doi.org/10.22146/ijc.39712>
14. Gopalakrishnan, Y.; Al-Gheethi, A.; Abdul Malek, M.; Marisa Azlan, M.; Al-Sahari, M.; Radin Mohamed, R.M.S.; Alkhadher, S.; Noman, E. Removal of basic brown 16 from aqueous solution using durian shell adsorbent, optimisation and techno-economic analysis. Sustainability, 2020, 12(21), 8928, pp. 1–22. DOI: <https://doi.org/10.3390/su12218928>
15. Sudrajat, H.; Susanti, A.; Putri, D.K.Y.; Hartuti, S. Mechanistic insights into the adsorption of methylene blue by particulate durian peel waste in water. Water Science and Technology, 2021, 84(7), pp. 1774–1792. DOI: <http://doi.org/10.2166/wst.2021.361>
16. Jawad, A.H.; Kadhum, A.M.; Ngoh, Y.S. Applicability of dragon fruit (*Hylocereus polyrhizus*) peels as low-cost biosorbent for adsorption of methylene blue from aqueous solution: kinetics, equilibrium and thermodynamics studies. Desalination and Water Treatment, 2018, 109, pp. 231–240. DOI: <https://doi.org/10.5004/dwt.2018.21976>
17. Lim, L.B.L.; Priyantha, N.; Latip, S.A.A.; Lu, Y.C.; Mahadi, A.H. Converting *Hylocereus undatus* (white dragon fruit) peel waste into a useful potential adsorbent for the removal of toxic Congo red dye. Desalination and Water Treatment, 2020, 185, pp. 307–317. DOI: <https://doi.org/10.5004/dwt.2020.25390>

18. Priyantha, N.; Lim, L.B.L.; Dahri, M.K. Dragon fruit skin as a potential biosorbent for the removal of methylene blue dye from aqueous solution. *International Food Research Journal*, 2015, 22(5), pp. 2141–2148. [http://ifrj.upm.edu.my/22%20\(05\)%202015/\(55\).pdf](http://ifrj.upm.edu.my/22%20(05)%202015/(55).pdf)
19. Thi, H.A.; Phuc, L.T.; Van Trong, N.; Thuy, T.T.T. Synthesis of materials from agricultural wastes combined with Fe<sub>3</sub>O<sub>4</sub> for methylene blue adsorption and application to treat organic pollutants in water samples. *Vietnam Journal of Chemistry*, 2024, 62(1), pp. 68–77. DOI: <https://doi.org/10.1002/vjch.202300120>
20. Dave, S.R.; Dave, V.A.; Tipre, D.R. Coconut husk as a biosorbent for methylene blue removal and its kinetics study. *Advances in Environmental Research*, 2012, 1(3), pp. 223–236. DOI: <http://doi.org/10.12989/aer.2012.1.3.223>
21. Wong, Y.C.; Senan, M.S.R.; Atiqah, N.A. Removal of methylene blue and malachite green dye using different form of coconut fibre as absorbent. *Journal of Basic & Applied Sciences*, 2013, 9, pp. 172–177. DOI: <http://doi.org/10.6000/1927-5129.2013.09.23>
22. Parvin, S.; Rahman, M.W.; Saha, I.; Alam, M.J.; Khan, M.M.R. Coconut tree bark as a potential low-cost adsorbent for the removal of methylene blue from wastewater. *Desalination and Water Treatment*, 2019, 146, pp. 385–392. DOI: <https://doi.org/10.5004/dwt.2019.23598>
23. Jawad, A.H.; Razuan, R.; Appaturi, J.N.; Wilson, L.D. Adsorption and mechanism study for methylene blue dye removal with carbonized watermelon (*Citrullus lanatus*) rind prepared via one-step liquid phase H<sub>2</sub>SO<sub>4</sub> activation. *Surfaces and Interfaces*, 2019, 16, pp. 76–84. DOI: <https://doi.org/10.1016/j.surfin.2019.04.012>
24. Shukla, S.; Khan, R.; Srivastava, M.M.; Zahmatkesh, S. Valorization of waste watermelon rinds as a bio-adsorbent for efficient removal of methylene blue dye from aqueous solutions. *Applied Biochemistry and Biotechnology*, 2023, 196, pp. 2534–2548. DOI: <http://doi.org/10.1007/s12010-023-04448-3>
25. Zhang, Z.; Xu, L.; Liu, Y.; Feng, R.; Zou, T.; Zhang, Y.; Kang, Y.; Zhou, P. Efficient removal of methylene blue using the mesoporous activated carbon obtained from mangosteen peel wastes: kinetic, equilibrium, and thermodynamic studies. *Microporous and Mesoporous Materials*, 2021, 315, pp. 110904. DOI: <https://doi.org/10.1016/j.micromeso.2021.110904>
26. Jawad, A.H.; Saber, S.E.M.; Abdulhameed, A.S.; Reghioua, A.; AlOthman, Z.A.; Wilson, L.D. Mesoporous activated carbon from mangosteen (*Garcinia mangostana*) peels by H<sub>3</sub>PO<sub>4</sub> assisted microwave: optimization, characterization, and adsorption mechanism for methylene blue dye removal. *Diamond and Related Materials*, 2022, 129, pp. 109389. DOI: <https://doi.org/10.1016/j.diamond.2022.109389>
27. Priatni, S.; Pradita, A. Stability study of betacyanin extract from red dragon fruit (*Hylocereus polyrhizus*) peels. *Procedia Chemistry*, 2015, 16, pp. 438–444. DOI: <https://doi.org/10.1016/j.proche.2015.12.076>
28. Diagboya, P.N.; Odagwe, A.; Oyem, H.H.; Omoruyi, C.; Osabohien, E. Adsorptive decolorization of dyes in aqueous solution using magnetic sweet potato (*Ipomoea batatas* L.) peel waste. *RSC Sustainability*, 2024, 2(3), pp. 686–694. DOI: <https://doi.org/10.1039/d3su00410d>
29. Sivashankar, R.; Thirunavukkarasu, A.; Nithya, R.; Kanimozhi, J.; Sathya, A.B.; Sivasubramanian, V. Sequestration of methylene blue dye from aqueous solution by magnetic biocomposite: three level Box–Behnken experimental design optimization and kinetic studies. *Separation Science and Technology*, 2020, 55(10), pp. 1752–1765. DOI: <https://doi.org/10.1080/01496395.2019.1607382>
30. Dbik, A.; El Messaoudi, N.; Bentahar, S.; El Khomri, M.; Lacherai, A.; Faska, N. Optimization of methylene blue adsorption on agricultural solid waste using Box–Behnken design (BBD) combined with response surface methodology (RSM) modeling. *Biointerface Research in Applied Chemistry*, 2022, 12(4), pp. 4567–4583. DOI: <https://doi.org/10.33263/BRIAC124.45674583>
31. APHA, AWWA, WEF, Standard Methods for the Examination of Water and Wastewater. Method 5220C - Closed Reflux, Titrimetric Method. APHA Press: Washington D.C., 1999, pp. 392–394. DOI: <https://doi.org/10.2105/SMWW.2882.103>
32. Wang, H.; Wang, P.; Kasapis, S.; Truong, T. Pomelo (*Citrus grandis* L.) peels as effective sorbents for diverse gel matrices: the influence of particle size and powder concentration. *Journal of Food Engineering*, 2024, 370, pp. 111966. DOI: <https://doi.org/10.1016/j.jfoodeng.2024.111966>
33. Ong, S.-T.; Tan, S.-Y.; Khoo, E.-C.; Lee, S.-L.; Ha, S.-T. Equilibrium studies for Basic blue 3 adsorption onto durian peel (*Durio zibethinus Murray*). *Desalination and Water Treatment*, 2012, 45(1–3), pp. 161–169. DOI: <https://doi.org/10.1080/19443994.2012.692037>
34. Channei, D.; Thammaacheep, P.; Jannoey, P. Utilizing banana peel in conjunction with TiO<sub>2</sub> photocatalyst for the efficient decolorization of malachite green. *Chemical Physics Impact*, 2024, 8, pp. 100629. DOI: <https://doi.org/10.1016/j.chphi.2024.100629>
35. Yahaya, N.P.; Ali, I.; Modu, K.A.; Adamu, S. Adsorption study of methylene blue onto power activated carbon prepared from ananas comosus peels. *Nanochemistry Research*, 2023, 8(4), pp. 231–242. DOI: <https://doi.org/10.22036/NCR.2023.04.01>
36. Ahmad, M.A.; Ahmad, N.; Bello, O.S. Modified durian seed as adsorbent for the removal of methyl red dye from aqueous solutions. *Applied Water Science*, 2015, 5, pp. 407–423. DOI: <https://doi.org/10.1007/s13201-014-0208-4>

37. Ghoohestani, E.; Samari, F.; Homaei, A.; Yosuefinejad, S. A facile strategy for preparation of Fe<sub>3</sub>O<sub>4</sub> magnetic nanoparticles using Cordia myxa leaf extract and investigating its adsorption activity in dye removal. Scientific Reports, 2024, 14(1), 84, pp. 1–15. DOI: <https://doi.org/10.1038/s41598-023-50550-1>
38. Narasimharao, K.; Al-Thabaiti, S.; Rajor, H.K.; Mokhtar, M.; Alsheshri, A.; Alfaifi, S.Y.; Siddiqui, S.I.; Abdulla, N.K. Fe<sub>3</sub>O<sub>4</sub>@ date seeds powder: A sustainable nanocomposite material for wastewater treatment. Journal of Materials Research and Technology, 2022, 18, pp. 3581–3597. DOI: <https://doi.org/10.1016/j.jmrt.2022.03.176>
39. Dang, L.-T.-C.; Phan, H.-V.-T.; Dao, M.-T.; Dang, T.-T.; Suvokhiaw, S.; Do, N.-T.; Nguyen T.-A.-M.; Nguyen, V.-K.; Hoang, L.-T.-T.-T. Facile synthesis of a 3D magnetic graphene oxide/Fe<sub>3</sub>O<sub>4</sub>/banana peel-derived cellulose composite aerogel for the efficient removal of tetracycline. RSC Advances, 2024, 14(46), pp. 34457–34470. DOI: <https://doi.org/10.1039/d4ra04942j>
40. Argun, M.E.; Güclü, D.; Karatas, M. Adsorption of reactive blue 114 dye by using a new adsorbent: pomelo peel. Journal of Industrial and Engineering Chemistry, 2014, 20(3), pp. 1079–1084. DOI: <https://doi.org/10.1016/j.jiec.2013.06.045>
41. Asbollah, M.A.; Sahid, M.S.M.; Shahrin, E.W.E.S.; Narudin, N.A.H.; Kusrini, E.; Shahri, N.N.M.; Hobley, J.; Usman, A. Dynamics and thermodynamics for competitive adsorptive removal of methylene blue and rhodamine B from binary aqueous solution onto durian rind. Environmental Monitoring and Assessment, 2022, 194(9), pp. 645. DOI: <https://doi.org/10.1007/s10661-022-10332-0>
42. El-Nafaty, U.A.; Muhammad, I.M.; Abdulsalam, S. Biosorption and kinetic studies on oil removal from produced water using banana peel. Civil and Environmental Research, 2013, 3(7), pp. 125–136. <https://core.ac.uk/download/pdf/234677596.pdf>
43. Allafchian, A.; Mousavi, Z.S.; Hosseini, S.S. Application of cress seed musilage magnetic nanocomposites for removal of methylene blue dye from water. International Journal of Biological Macromolecules, 2019, 136, pp. 199–208. DOI: <https://doi.org/10.1016/j.ijbiomac.2019.06.083>
44. Ebrahimian Pirbazari, A.; Saberikhah, E.; Habibzadeh Kozani, S.S. Fe<sub>3</sub>O<sub>4</sub>–wheat straw: preparation, characterization and its application for methylene blue adsorption. Water Resources and Industry, 2014, 7-8, pp. 23–37. DOI: <https://doi.org/10.1016/j.wri.2014.09.001>
45. Aryee, A.A.; Zhang, R.; Liu, H.; Han, R.; Li, Z.; Qu, L. Application of magnetic peanut husk for methylene blue adsorption in batch mode. Desalination and Water Treatment, 2020, 194, pp. 269–279. DOI: <https://doi.org/10.5004/dwt.2020.25862>
46. Lawagon, C.P.; Amon, R.E.C. Magnetic rice husk ash 'cleanser' as efficient methylene blue adsorbent. Environmental Engineering Research, 2020, 25(5), pp. 685–692. DOI: <https://doi.org/10.4491/eer.2019.287>